

NRQED and Next-to-Leading Hyperfine Splitting in Positronium

P. Labelle, S.M. Zebarjad and C.P. Burgess

Physics Department, McGill University

3600 University Street, Montréal, Québec, Canada, H3A 2T8.

Abstract

We compute the next-to-leading, $O(m\alpha^5)$, contribution to the hyperfine splitting in positronium within the framework of NRQED. When applied to the ground state, our calculation reproduces known results, providing a further test of NRQED techniques. Besides providing a very simple method of calculation of the standard result, we also obtain new expressions for excited states of positronium with negligible additional effort. Our calculation requires the complete next-to-leading matching of the lowest-dimension NRQED four-fermi couplings, which we publish here for the first time.

1. Introduction and Summary

The detailed comparisons between the heroic precision calculations using Quantum Electrodynamics (QED) and equally heroic precision measurements represent one of the pinnacles of twentieth-century physics. On the theoretical side, comparisons involving the energy levels of bound states, such as hydrogen or positronium, pose a particular challenge. This is because of the necessity of incorporating the small radiative corrections of relativistic QED into the nonperturbative treatment required for the bound state itself. Important conceptual progress in handling bound states in QED was made several years ago [1] with the development of nonrelativistic QED (NRQED), which consists of an application of effective-field-theory ideas to atomic physics applications of QED.

NRQED starts with the recognition that much of the complication of QED bound-state calculations arises because the fine-structure constant,¹ $\alpha = e^2/4\pi$, enters into observables in two conceptually different ways. First, α enters as the small parameter which controls the higher-order QED radiative corrections. Second, α enters from the appearance in these calculations of three separate scales: the electron mass, m , the bound-state momentum, mv , and the bound-state energy, mv^2 , once it is recognized that $v = O(\alpha)$ in the bound state. While much of the higher-order QED radiative corrections involve scales at, or above, m , where relativistic kinematics is important, the complications associated with handling the bound states all arise at the lower two scales, mv and mv^2 .

NRQED takes advantage of this hierarchy of scales to efficiently separate the radiative corrections from the bound-state physics. First one accurately integrates out all physics associated with momenta $p \gtrsim O(m)$, obtaining an effective theory of nonrelativistic particles whose interactions are organized according to their suppression by powers of the two independent small parameters, α and v . This effective theory is then used to systematically compute bound-state properties, at which point v becomes of order α . Keeping v and α independent until this last step makes the bookkeeping more straightforward. The additional bonus is that bound state calculations are much easier to do within the effective

¹ We use throughout units for which $\hbar=c=1$.

theory because its nonrelativistic framework permits the direct application of well-tested techniques based on Schrödinger's equation.

Any effective field theory relies on the existence of a hierarchy of scales, say $M_1 \ll M_2$, in a physical problem. The heart of the effective theory's utility lies in its powercounting rules, which identify how to systematically isolate the complete contributions to any observable to any fixed order in the small ratio, M_1/M_2 . NRQED is no exception in this regard, with the powercounting rules identifying the suppression of observables in powers of $v \sim \alpha$. It is the recent development of NRQED power-counting rules [2], which now makes it possible to directly identify the $O(\alpha^n)$ contributions to any atomic-physics observable. These rules have recently been demonstrated in practice in an illustrative calculation of the Lamb shift [3].

Although contributions order by order in α can also be obtained by other methods, the virtue of NRQED lies in its simplicity, since this potentially brings more complicated calculations into the domain of the feasible. Besides permitting the very simple extension of low-order results to bound states involving particles of other spins [4], NRQED's simplicity has very recently been exploited to give the first-ever analytical calculation of the last previously uncomputed $O(m\alpha^6)$ contribution to positronium hyperfine splitting [5].

In the present paper we continue this process in other directions. Since the power of effective field theory methods are best seen once one goes beyond leading order in small parameters, we present here an NRQED calculation of the complete contributions to the positronium hyperfine structure at next-to-leading order, $O(m\alpha^5)$. The result we obtain for the ground state hyperfine splitting agrees with previous results [6]. However our results are easily extended to the hyperfine splitting of excited states having arbitrary quantum numbers n and ℓ . These agree with previous results [7] for arbitrary n but $\ell = 0$, but to our knowledge ours is the first calculation which is applicable to general n and ℓ .

Our goal in presenting this calculation is twofold. One of our aims is to make NRQED accessible to a wider community. Detailed calculations which can be compared to known results partly act as a vehicle for explaining how NRQED works. On the other hand, some of our results are new and interesting in their own right. Our new results come in

two forms. First, an intermediate step in our calculation is the matching from QED to NRQED at next-to-leading order in α . Only part of this matching is already available in the literature, and the remainder, which we publish here for the first time, will have applications to many other higher-precision NRQED calculations. In addition, our results for the hyperfine structure of the excited states of positronium are also new.

We organize our presentation as follows. In §2 we briefly review the NRQED lagrangian, including a discussion of the matching which is required to obtain some of the NRQED couplings to next-to-leading order in α . We first summarize the next-to-leading matchings which are already given in the literature, followed by a calculation of a final class of matchings which have not been previously published, but which are required to obtain the hyperfine structure to the order we require. §3 gives a quick summary of NRQED powercounting, as obtained in ref. [2]. These powercounting rules are then used to systematically identify all possible contributions to the $O(m\alpha^5)$ hyperfine splitting. The main result of this section is that the complete $O(m\alpha^5)$ contribution is obtained in NRQED using precisely the same graphs as for the $O(m\alpha^4)$ contribution, but with coupling constants which are matched to relativistic QED to higher order in α . These results are finally brought together in §4, where we present our results for the hyperfine splitting. We do this for both the ground state and for the excited states of positronium.

2. NRQED

We start with the lagrangian density of NRQED as applied to nonrelativistic electrons and positrons, which is obtained from full QED by integrating out all virtual physics at scales greater than the electron mass, $\Lambda \gtrsim m$.

2.1) The Lagrangian

The fields representing the low energy degrees of freedom are ψ , χ and A_μ , which respectively represent the nonrelativistic electron, the nonrelativistic positron and photons with energy less than m . The lagrangian is: $\mathcal{L} = \mathcal{L}_{\text{photon}} + \mathcal{L}_{2\text{-Fermi}} + \mathcal{L}_{4\text{-Fermi}} + \dots$, with:

$$\begin{aligned}
\mathcal{L}_{2\text{-Fermi}} &= \psi^\dagger \left[iD_t + \frac{\mathbf{D}^2}{2m} + \frac{\mathbf{D}^4}{8m^3} + c_1 \boldsymbol{\sigma} \cdot \mathbf{B} \right. \\
&\quad \left. + c_2 (\mathbf{D} \cdot \mathbf{E} - \mathbf{E} \cdot \mathbf{D}) + c_3 \boldsymbol{\sigma} \cdot (\mathbf{D} \times \mathbf{E} - \mathbf{E} \times \mathbf{D}) + \dots \right] \psi + (\psi \rightarrow \chi), \\
\mathcal{L}_{4\text{-Fermi}} &= c_4 \psi^\dagger (\boldsymbol{\sigma} \sigma_2) \chi^* \cdot \chi^T (\sigma_2 \boldsymbol{\sigma}) \psi + c_5 \psi^\dagger (\sigma_2) \chi^* \chi^T (\sigma_2) \psi \\
&\quad + c_6 \left[\psi^\dagger (\sigma_2 \boldsymbol{\sigma}) \mathbf{D}^2 \chi \cdot \chi^\dagger (\sigma_2 \boldsymbol{\sigma}) \psi \right] + \dots, \\
\mathcal{L}_{\text{photon}} &= \frac{1}{2} (\mathbf{E}^2 - \mathbf{B}^2) + c_9 A_0(\mathbf{k}) \frac{\mathbf{k}^4}{m^2} A_0(\mathbf{k}) \\
&\quad - c_{10} A_i(\mathbf{k}) \frac{\mathbf{k}^4}{m^2} A_j(\mathbf{k}) \left(\delta_{ij} - \frac{k_i k_j}{\mathbf{k}^2} \right) + \dots.
\end{aligned} \tag{1}$$

Here $D_t = \partial_t - iqeA_0$ and $\mathbf{D} = \nabla - iqe\mathbf{A}$, where $q = -1$ for electrons and $q = +1$ for positrons. $\boldsymbol{\sigma}$ represents the usual Pauli spin matrices. The Feynman rules corresponding to this lagrangian are listed in Figure (1).

2.2) Matching at Leading-Order

The various coefficients, c_i , appearing in this expression are calculable functions of α and m which are obtained by integrating out scales larger than m using QED. They may be conveniently determined by computing scattering processes for free electrons and positrons using both full QED and the NRQED lagrangian, Eqs. (1). Equating the results to a fixed order in α and v completely determines the constants c_i to this order.

Performing this operation at tree level in QED gives the lowest-order results in α [1]:

$$c_1^{(0)} = \frac{qe}{2m}, \quad c_2^{(0)} = \frac{qe}{8m^2}, \quad c_3^{(0)} = \frac{iqe}{8m^2}, \quad c_4^{(0)} = -\frac{\pi\alpha}{m^2}, \tag{2}$$

and

$$c_5^{(0)} = c_6^{(0)} = c_9^{(0)} = c_{10}^{(0)} = 0. \tag{3}$$

² We omit the four fermion terms proportional to c_7 and c_8 which are listed in ref. [2], because they are redundant in the sense that they may be expressed in terms of those we display.

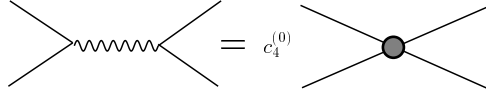


Figure (2)

The matching which determines $c_4^{(0)}$.

To see how these arise consider, for example, the contribution to the effective four-fermi couplings c_4 and c_5 . These four-fermi operators reproduce in NRQED the effects of the tree-level s -channel annihilation graph of QED, given in Figure (2). This must be reproduced by an effective interaction because the photon which is exchanged must necessarily involve four-momenta of order m , and so cannot appear in the effective theory.

In performing the matching, we evaluate all diagrams at threshold — *i.e.* with vanishing external three momentum in the center of mass frame of the electron-positron pair. We use this choice of external momentum purely for convenience, and the matching could equally well be performed with non-zero (but nonrelativistic) three-momenta for the electron and positron, giving precisely the same NRQED coefficients. Notice also that care must be taken that the scattering amplitude is normalized in the same way when comparing the QED and NRQED results, since the covariant normalization of relativistic spinors involves additional factors of $\sqrt{2E}$ compared to nonrelativistic applications.

The contributions to the coefficients c_4 and c_5 are distinguished from one another by separately evaluating the QED amplitudes for the electron-positron spins combined into a spin triplet ($S = 1 \leftrightarrow c_4$) or a spin singlet ($S = 0 \leftrightarrow c_5$). It follows that $c_5^{(0)}$ must vanish since the spin-singlet combination of the electron and positron is forbidden by charge conjugation invariance from receiving a contribution from the s -channel annihilation graph of Fig. (2).

Although the t -channel photon-exchange graph is also involved in electron-positron scattering at tree level in QED, it does not contribute to either $c_4^{(0)}$ or $c_5^{(0)}$. Indeed, for nonrelativistic electrons and photons the energy of the exchanged photon is much below the electron mass and so this scattering is described by the same t -channel graph in NRQED.

As a result tree-level t -channel photon exchange does not contribute to any of the NRQED four-fermi operators in the matching process.

It bears emphasis that the matching calculation does not involve any bound states at all, since it is done using only the scattering of free electrons and positrons. Matching is also the only stage of the calculation which involves QED diagrams. Once the couplings of the NRQED lagrangian are obtained in this way, only they are used in the subsequent bound state part of the calculation. This separation of the matching from the bound state calculations lies at the heart of NRQED's simplicity. For example, this separation permits the use of different gauges in the relativistic and nonrelativistic parts of the calculation, since the gauge choice when using NRQED is independent of the gauge used in QED, so long as one computes only gauge-invariant quantities. This permits the convenience of using a covariant gauge, like Feynman gauge, in the QED part of the calculation, while keeping Coulomb gauge for NRQED calculations.

2.3) Matching at Next-to-Leading Order

More accurate calculations, such as those of interest in this paper, require the next-to-leading corrections to the coefficients of Eqs. (2). Some of these corrections are already given in the literature, and some we compute here for the first time. Since our new calculations are for the coefficients of the four-fermi coupling constants, c_4 and c_5 , we discuss the corrections to these quantities in some detail, and give only a brief summary of the higher-order corrections to both $\mathcal{L}_{\text{photon}}$ and $\mathcal{L}_{2\text{-Fermi}}$. We write $c_i = c_i^{(0)} + c_i^{(1)} + \dots$ with $c_i^{(0)}$ as given in the previous section, and now concentrate on computing the next corrections, $c_i^{(1)}$.

Among the simplest higher-order corrections to the NRQED lagrangian, Eq. (1), are the contributions to $\mathcal{L}_{\text{photon}}$. To lowest order these are produced by vacuum polarization, which gives:

$$c_9^{(1)} = c_{10}^{(1)} = \frac{\alpha}{15\pi}. \quad (4)$$

Similarly, QED one-loop vertex corrections modify the couplings in $\mathcal{L}_{2\text{-Fermi}}$, to give

[8], [9]:

$$c_1^{(1)} = \frac{qe}{2m} \left(\frac{\alpha}{2\pi} \right), \quad c_2^{(1)} = -\frac{qe}{8m^2} \left(\frac{\alpha}{\pi} \right) \left[\ln \left(\frac{2\Lambda}{m} \right) - \frac{20}{9} \right], \quad c_3^{(1)} = \frac{iqe}{8m^2} \left(\frac{\alpha}{\pi} \right). \quad (5)$$

Here Λ is the ultraviolet cutoff used to regulate NRQED loop graphs which arise when matching. In any calculation of physical properties, such divergences cancel amongst themselves, or against explicit cutoff dependence which arises from divergences in NRQED loop graphs.

We now turn to the next-to-leading corrections to $\mathcal{L}_{4-\text{Fermi}}$. These corrections may be divided into the following three classes according to the topology of the one-loop QED graphs which are involved:

- *One-Photon Annihilation:* These corrections consist of QED graphs which describe one-loop corrections to the tree-level process of the s -channel exchange of a single virtual photon. As before t -channel exchange of a single virtual photon does not contribute corrections to $\mathcal{L}_{4-\text{Fermi}}$.
- *Two-Photon Annihilation:* These consist of the QED ‘box’ graphs which describe the s -channel exchange of two virtual photons.
- *t -Channel Two-Photon Exchange:* The final class consists of QED box graphs which describe the t -channel exchange of two virtual photons. Although t -channel one-photon exchange does not contribute to NRQED four-fermion interactions, t -channel two-photon exchange *does* contribute because there is a region of phase space for which the loop momentum is larger than the electron mass, and so which does not appear in the corresponding two-photon exchange graphs of NRQED. The corresponding physics is therefore put back into the effective field theory through the NRQED four-fermi interactions.

We now describe, in turn, the matching due to each of these classes of graphs. While the contributions to $c_4^{(1)}$ and $c_5^{(1)}$ due to the first two of these may be found in the literature [8], [9], those due to the third class we present here for the first time.

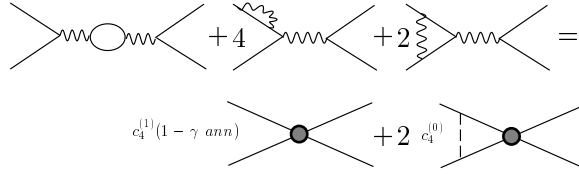


Figure (3)

The graphs which give the one-photon annihilation contribution to $c_4^{(1)}$.

Matching due to one-loop corrections to single-photon annihilation are described by the graphs of Figure (3). The contributions to the scattering amplitude of electrons and positrons at threshold from the QED graphs on the left-hand-side of the equality in this figure must be equated to the contributions of the NRQED graphs on the right-hand-side. Separately evaluating the QED graphs for a spin-singlet and spin-triplet e^+e^- state, and solving the resulting equalities for $c_4^{(1)}$ and $c_5^{(1)}$ then gives [8], [9]:

$$c_4^{(1)}(1-\gamma \text{ ann}) = \frac{44\alpha^2}{9m^2}, \quad c_5^{(1)}(1-\gamma \text{ ann}) = 0. \quad (6)$$

Just as for tree-level matching, the contribution to the spin-singlet coupling, c_5 , vanishes by virtue of charge-conjugation invariance.

Although all possible one-loop s -channel single-photon exchange QED graphs appear on the left-hand-side of Fig. (3), the same is not true of the NRQED graphs appearing on the right-hand-side. An important issue is therefore how to determine which NRQED graphs must be included to any given order in the matching process. The simplest way to do this is to imagine performing the matching slightly off-threshold, *i.e.* with the external particles having a small velocity in the center of mass frame. As mentioned earlier, this does not affect the value of the NRQED coefficients. Which NRQED diagram must be kept is then decided by counting powers of α and v , with $v \sim \alpha$ kept in mind for bound-state applications.

For example, for the present purposes of computing the $O(m\alpha^5)$ hyperfine splitting, we show in §3 that we require both c_4 and c_5 to next-to-leading order, $O(\alpha^2)$. This implies both of these couplings must be matched to QED with an accuracy up to order α^2v^0 . The

NRQED diagram proportional to $c_4^{(1)}$ is of order $\alpha^2 v^0$. The loop diagram involving the exchange of one Coulomb photon contributes to order³ α^2/v and cancels a similar term in the QED one loop vertex correction. At threshold, the $1/v$ contribution becomes⁴ a $1/\lambda$ infrared divergence which, cancels a similar term in the QED diagram. Because the coefficients of the effective theory describes only high-energy virtual effects in QED, it is a general result that matching always produces infrared finite values for them.

Notice also that all other NRQED loop graphs which could appear on the right-hand-side necessarily involve additional powers of the electron or positron velocity, v , and so give contributions to c_4 which are smaller than $O(\alpha^2)$. For example, since the Feynman rule for the emission of a soft photon is proportional to $ep/m = ev$, the loop graph obtained by dressing a four-fermi interaction with a soft-photon line rather than a Coulomb line, contributes a term of order $\alpha v^2 c_4^{(0)}$ to the scattering amplitude, representing a correction to c_4 which is of order α^4 in any bound-state application. In this way it may be seen that only the Coulomb-exchange NRQED loop need be kept in Fig. (3).

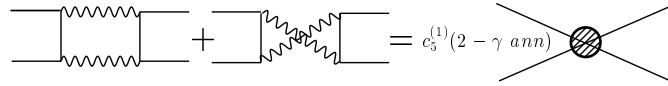


Figure (4)

Diagrams which contribute to two-photon annihilation contributions to $c_5^{(1)}$.

We next turn to the QED box graphs describing s -channel electron-positron annihilation into two virtual photons, Figure (4). The matching appropriate for these graphs gives [8], [9]:

$$c_4^{(1)}(2-\gamma \text{ ann}) = 0, \quad c_5^{(1)}(2-\gamma \text{ ann}) = \left(\frac{\alpha^2}{m^2}\right) (2 - 2 \ln 2 + i\pi). \quad (7)$$

This time charge-conjugation invariance forbids a contribution to the spin-triplet operator, c_4 .

³ This diagram is proportional to $\alpha^2 \int d^3 k / ((\vec{p}^2 - \vec{k}^2 + i\epsilon)(\vec{k} - \vec{p})^2) \simeq \alpha^2/p$ where $p = mv$ is the external momentum.

⁴ We regulate all such infrared divergences by including a photon mass, λ , into photon propagators.

Notice, in this last equation, that the one-loop contribution to c_5 , has both a real and imaginary part. This imaginary part causes the low-energy hamiltonian not to be hermitian. The resulting loss of unitarity in the time evolution is just what is required to describe the depletion of electrons and positrons due to their mutual annihilation into real photons. Since annihilation is a high-energy effect, it appears in NRQED as an effective four-fermi operator. This imaginary part may be used to compute the decay rate for positronium bound states by calculating the imaginary part it implies for the bound state energy eigenvalue, E . The decay rate for bound state is then given by the familiar relation, $\Gamma = -2 \text{Im}(E)$.

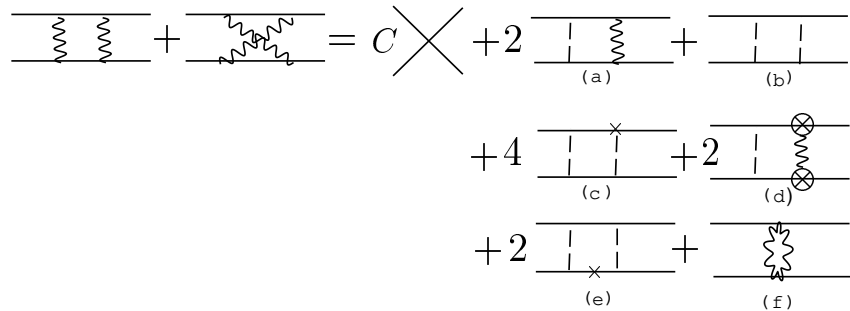


Figure (5)

The one-loop t -channel matching diagrams.

We now turn to the contribution to c_4 and c_5 due to the t -channel two-photon QED exchange graphs, given in Figure (5). Here the diagram proportional to C is meant to represent the vertex, $c_4^{(1)}$, when the diagrams are evaluated in a spin 1 state, and $c_5^{(1)}$ when the diagram is evaluated in a spin 0 state. It is straightforward to verify that only the given NRQED graphs can contribute to these coefficients to $O(\alpha^2)$ when $v \sim \alpha$.

In order to determine $c_4^{(1)}$ and $c_5^{(1)}$ separately, we must include all of the spin-independent NRQED diagrams in the matching. This is actually more work than is required purely for the purposes of calculating the hyperfine splitting, since only the difference $c_4^{(1)} - c_5^{(1)}$ enters into this quantity. Since the spin-independent graphs cancel in this difference, it suffices to just compute spin-dependent graphs if one is strictly interested only in the hyperfine

splitting. However, we present here the separate matching for both c_4 and c_5 , since these two coefficients must be known separately for other applications, such as for the complete $O(m\alpha^5)$ shift of the positronium energy levels.

Evaluating the left-hand side of Fig. (5) (the QED graphs) for a spin-triplet electron-positron configuration gives, after a straightforward calculation:

$$(\text{QED})_{S=1} = \alpha^2 \left[\frac{-2\pi m}{\lambda^3} + \frac{11\pi}{12\lambda m} + \frac{4}{3m^2} + \frac{2}{m^2} \ln \left(\frac{\lambda}{m} \right) \right]. \quad (8)$$

Recall λ is the infrared-regulating photon mass.

Using the NRQED Feynman rules to calculate the right-hand-side of Fig. (5) gives the following contributions. The only spin-dependent NRQED diagram, part (d) of Figure (5), gives:

$$\begin{aligned} (\text{NRQED})_{S=1}(d) &= 2 \int \frac{d^3\mathbf{p}}{(2\pi)^3} \left(\frac{-ie\mathbf{p} \times \boldsymbol{\sigma}_1}{2m} \right)_i \left(\frac{-ie\mathbf{p} \times \boldsymbol{\sigma}_2}{2m} \right)_j \left(\frac{-1}{\mathbf{p}^2 + \lambda^2} \right) \\ &\quad \times \left(\delta_{ij} - \frac{\mathbf{p}_i \mathbf{p}_j}{\mathbf{p}^2 + \lambda^2} \right) \left(\frac{-m}{\mathbf{p}^2} \right) \left(\frac{-e^2}{\mathbf{p}^2 + \lambda^2} \right) \\ &= \frac{8\alpha^2}{3m} \left(\int \frac{dp \mathbf{p}^2}{(\mathbf{p}^2 + \lambda^2)^2} \right) \\ &= \frac{2\pi\alpha^2}{3m\lambda}, \end{aligned} \quad (9)$$

where the overall factor of 2 in the first line takes into account the two possible ways in which the NRQED diagram can be drawn.

Similarly, diagram (f) of Fig. (5) gives:

$$\begin{aligned} (\text{NRQED})_{S=1}(f) &= \int \frac{d^3\mathbf{p}}{(2\pi)^3} \left(\frac{e^2}{2m} \right) \left(\frac{e^2}{2m} \right) \frac{1}{\sqrt{\mathbf{p}^2 + \lambda^2}} \\ &\quad \times \left(\delta_{ij} - \frac{\mathbf{p}_i \mathbf{p}_j}{\mathbf{p}^2 + \lambda^2} \right) \frac{-1}{2\sqrt{\mathbf{p}^2 + \lambda^2} \sqrt{\mathbf{p}^2 + \lambda^2}} \left(\delta^{ij} - \frac{\mathbf{p}^i \mathbf{p}^j}{\mathbf{p}^2 + \lambda^2} \right) \\ &= \frac{\alpha^2}{m^2} \left[\frac{28}{15} - 2 \ln 2 + \ln \left(\frac{\lambda}{\Lambda} \right) \right]. \end{aligned} \quad (10)$$

All the other NRQED diagrams can be calculated in a similar manner. The final result for the sum of the NRQED diagrams, evaluated in a spin-triplet state is:

$$(\text{NRQED})_{S=1} = -2 c_4^{(1)}(t\text{-ch}) + \alpha^2 \left[\frac{-2\pi m}{\lambda^3} + \frac{11\pi}{12\lambda m} + \frac{28}{15m^2} - \frac{2}{m^2} \ln 2 + \frac{2}{m^2} \ln \left(\frac{\lambda}{\Lambda} \right) \right]. \quad (11)$$

Solving for $c_4(t\text{-ch})$ then gives the result:

$$c_4^{(1)}(t\text{-ch}) = - \left(\frac{\alpha^2}{m^2} \right) \left[\ln \left(\frac{\Lambda}{m} \right) - \frac{4}{15} + \ln 2 \right]. \quad (12)$$

An identical procedure applies to the $S = 0$ state. The QED graphs are then found to give:

$$(\text{QED})_{S=0} = \alpha^2 \left[\frac{-2\pi m}{\lambda^3} - \frac{21\pi}{12\lambda m} + \frac{16}{3m^2} + \frac{2}{m^2} \ln \left(\frac{\lambda}{m} \right) \right]. \quad (13)$$

For $S = 0$, part (d) of Fig. (5) now equals

$$(\text{NRQED})_{S=0}(d) = - \frac{2\pi\alpha^2}{\lambda m} \quad (14)$$

whereas the other NRQED diagrams are left unchanged because they are spin independent. The sum of the NRQED diagrams is then found to be

$$(\text{NRQED})_{S=0} = -2 c_5^{(1)}(t\text{-ch}) + \alpha^2 \left[\frac{-2\pi m}{\lambda^3} - \frac{21\pi}{12\lambda m} + \frac{28}{15m^2} - \frac{2}{m^2} \ln(2) + \frac{2}{m^2} \ln \left(\frac{\lambda}{\Lambda} \right) \right]. \quad (15)$$

The complete matching result from Fig. (5) then is

$$c_5^{(1)}(t\text{-ch}) = - \left(\frac{\alpha^2}{m^2} \right) \left[\ln \left(\frac{\Lambda}{m} \right) + \frac{26}{15} + \ln 2 \right]. \quad (16)$$

The complete one-loop contributions to the coefficients c_4 and c_5 are then given by combining the results from all three classes of graphs:

$$\begin{aligned} c_4^{(1)} &= c_4^{(1)}(1\text{-}\gamma \text{ ann}) + c_4^{(1)}(t\text{-ch}) = \frac{\alpha^2}{m^2} \left[-\ln \left(\frac{\Lambda}{m} \right) + \frac{232}{45} - \ln 2 \right] \\ c_5^{(1)} &= c_5^{(1)}(2\text{-}\gamma \text{ ann}) + c_5^{(1)}(t\text{-ch}) = \frac{\alpha^2}{m^2} \left[-\ln \left(\frac{\Lambda}{m} \right) + \frac{4}{15} - 3 \ln 2 + i\pi \right]. \end{aligned} \quad (17)$$

With the NRQED lagrangian now in hand, we next proceed with the determination of which graphs can contribute to the $O(m\alpha^5)$ hyperfine splitting in positronium.

3. Power Counting

The essence of any effective field theory is its powercounting rules, since these are what permits the systematic calculation of observables to any order in small ratios of scales. Unfortunately, power counting in NRQED is slightly more complicated than in many effective field theories because of the appearance of ‘ultrasoft’ photons. Recall that the charged particles in a QED bound state typically have momenta $p \sim m\alpha$ and energy $E \sim m\alpha^2$. Photons can therefore be emitted with momenta equal to *either* of these scales. Photons having momenta, k , (and energy, ω) of order $m\alpha$ (which we will refer to as ‘soft’) do not pose any problems for powercounting, but those having $k, \omega \sim m\alpha^2$ — the ‘ultrasoft’ ones — do. Physically, such ultrasoft photons represent the effects of retardation in the effective theory.

Fortunately, these ultrasoft photons have wavelengths which are also large compared to the size of the bound state, and so their effects can be organized into slightly more complicated powercounting rules using what amounts to a multipole expansion in their couplings to the charged particles. In the final analysis, this multipole expansion introduces extra suppression by powers of α into interaction vertices involving ultrasoft photons and their contribution to the hyperfine splitting starts at order $m\alpha^6$ [2].

3.1) General Powercounting Rules

When the dust settles, the powercounting result as applied to positronium has an appealingly simple form [2]. Consider computing a contribution to a positronium bound-state observable using the NRQED lagrangian, Eq. (1), in old-fashioned nonrelativistic Rayleigh-Schrödinger perturbation theory. Each term in this perturbation series can be expressed graphically, with time moving to the right, say, and with internal lines denoting the particles which contribute to the sum over intermediate states.

For NRQED, we use Coulomb gauge, which is the most efficient gauge for the study of nonrelativistic systems. In this gauge, there are two types of photon propagator, one corresponding to Coulomb photons (which are represented by dotted lines in the Feynman diagrams) and one corresponding to transverse photons (represented by wavy lines). The Coulomb photons are soft whereas the transverse photons can be either soft or ultra-soft. Soft transverse photons are represented by slanted lines in old-fashioned perturbation theory whereas soft transverse photons are represented by vertical lines (see [2] for more details). As mentioned above, the ultra-soft contributions can be shown to be beyond the order we are interested in this work, and we will therefore consider only soft transverse photons. When only soft photons are present – *i.e.* when retardation effects are neglected – all NRQED diagrams reduce to a set of instantaneous interactions, which can be Fourier transformed to local interactions in coordinate space separated by electron-positron propagators.

There are three quantities which determine the size of the contribution of any such graph to bound-state observables [2]. For any graph define N to be the number of electron-positron propagators separating the instantaneous interactions.⁵ The other two quantities are related to the powers of α and $1/m$ which appear in each of the coupling constants, c_i , of the NRQED lagrangian. Define, then, κ and n to be, respectively, the total number of powers of $1/m$ (or v) and α which appear in the vertices of the graph of interest.

Suppose N , κ and n are known for any particular NRQED graph. Then the contribution of this graph to the energy-level shift in positronium depends on m and α (modulo logarithms of α) through the combination $m\alpha^p$, where [2]:

$$p = 1 + \kappa + n - N. \tag{18}$$

Although the quantity N enters this expression with a negative sign, inserting additional interactions (and so increasing N) typically involves sufficient additional vertices to ensure that the net contribution to p increases and that the contribution from the diagram is therefore suppressed. The only exception to this statement is repeated insertions of the

⁵ N is denoted N_{TOP} in ref. [2].

Coulomb interaction, which increase both N and n by one but leaves κ unchanged (recall the Coulomb interaction does not contain any powers of inverse mass). Therefore, adding any number of Coulomb interactions to a given diagram leaves the value of p unchanged, indicating that one cannot perturb in the Coulomb interaction, which must be summed up to all orders. This is accomplished by using Schrödinger wavefunctions for the external lines of the bound state diagrams and the nonrelativistic Schrödinger-Coulomb propagator for intermediate states. On the other hand, it is easy to see that adding any other interaction increases the value of p since they always contain powers of $1/m$. There is therefore only a finite number of graphs which can contribute for any positive choice for p .

3.2) Applications to Hyperfine Splitting

We may now apply these powercounting arguments to the hyperfine splitting. An important simplifying feature appears in this specific application, since the hyperfine splitting compares the energies of two states having different net spin. As a result it suffices to consider only graphs for which at least one of the vertices involves a spin-dependent coupling.

To proceed, we start by recapping the powercounting which leads to the graphs which contribute to the $O(m\alpha^4)$ hyperfine splitting [4]. In this case we require $p = 4$, so $\kappa + n - N = 3$. Consider first the case $N = 0$. In this case we require all possible graphs containing a single instantaneous photon exchange, subject to the following two conditions: (i) at least one vertex is spin dependent; and (ii) $\kappa + n = 3$. The five classes of graphs which satisfy these two conditions are displayed in Figure (6). The coupling which appears in part (a) of this figure is c_1 , which appears twice, so inspection of Eq. (2) shows that the tree-level contribution, $c_1^{(0)}$, gives $\kappa = 2$ and $n = 1$, as required. The same is true for parts (b) — which is linear in $c_1^{(0)}$ — and (c) — which is proportional to $c_3^{(0)}$. Finally, parts (d) and (e) involve the four-fermi couplings, c_4 and c_5 , the largest of which also arises at tree-level, proportional to α/m^2 , again giving $\kappa = 2$, $n = 1$. It follows that these graphs contribute to $O(m\alpha^4)$ provided we use the leading-order contribution to their couplings. It is noteworthy that only the graphs of parts (a), (d) and (e) of Figure (6) contribute to

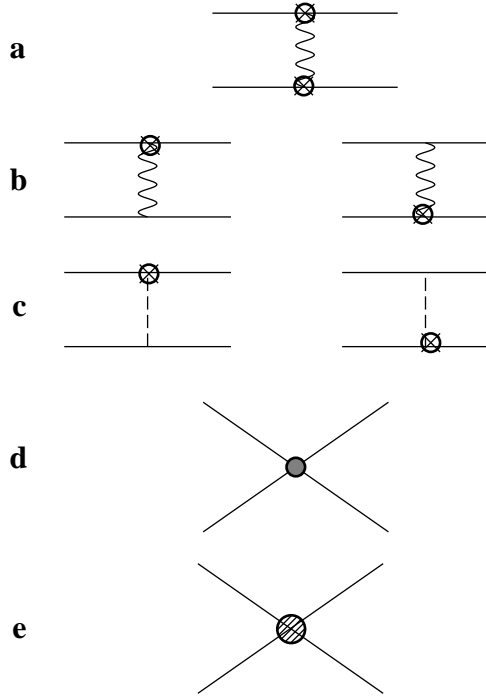


Figure (6)

The NRQED graphs which contribute to the hyperfine structure at order $m\alpha^4$.

the hyperfine splitting of the ground state, since all of the others vanish when evaluated in an s -wave configuration.

It now remains to consider the case $N > 0$. Having $N = 1$ implies including one more interaction in addition to the diagrams shown in Figure (3). It can be easily verified that any additional interaction (excluding, of course, the Coulomb interaction) increases the combination $\kappa + n$ by at least 3. For example, one can add a transverse photon coupled to two dipole vertices, introducing the square of the coefficient $c_1^{(0)} = qe/(2m)$. This increases κ by 2 and n by 1. The net change in p is therefore $3 - 1 = 2$ and the diagram contributes only to order $m\alpha^6$. Similarly, adding a Coulomb photon connected to a Coulomb and Darwin vertex increases κ by 2 and n by 1, whereas adding a relativistic kinetic vertex doesn't change n but increases κ by 3. Adding other interactions necessarily leads to, at best, $O(m\alpha^6)$.

This last argument has immediate implications for calculating the $O(m\alpha^5)$ hyperfine

structure. To this order all of the relevant graphs must still have $N = 0$. The next-to-leading result is therefore obtained from the *same* graphs, Figure (6), but using the next-to-leading order — *i.e.* $O(\alpha^2)$ — contributions to the coefficients, c_i . We next show in more detail how these corrections are computed for the case of the coefficients of the four-fermi interactions, $c_4^{(1)}$ and $c_5^{(1)}$.

4. Results

To compute the hyperfine splitting we evaluate the graphs of Figure (6) using Coulomb wavefunctions to describe the initial and final electron-positron lines. Consider, first, the hyperfine splitting for s -wave states. In this case only graphs (a), (d) and (e) of Fig. (6) contribute since the other two graphs contain one vector, $\boldsymbol{\sigma}$, which can't be dotted into any other vector if $\ell = 0$. We find

$$\begin{aligned}
\delta E_n(a) &= 2 \left(\frac{\alpha}{2\pi} \right) \int \frac{d^3\mathbf{p} d^3\mathbf{k}}{(2\pi)^3} \Psi^*(\mathbf{p}) \left(\frac{-ie(\mathbf{p} - \mathbf{k}) \times \boldsymbol{\sigma}_1}{2m} \right)_i \left(\frac{-ie((\mathbf{p} - \mathbf{k}) \times \boldsymbol{\sigma}_2)}{2m} \right)_j \\
&\quad \frac{-1}{(\mathbf{p} - \mathbf{k})^2} \left(\delta_{ij} - \frac{(\mathbf{p} - \mathbf{k})_i(\mathbf{p} - \mathbf{k})_j}{(\mathbf{p} - \mathbf{k})^2} \right) \Psi(\mathbf{k}) \\
&= 2 \left(\frac{\alpha}{2\pi} \right) \frac{2\pi\alpha}{3m^2} \langle \boldsymbol{\sigma}_1 \cdot \boldsymbol{\sigma}_2 \rangle |\Psi(0)|^2 \\
&= 2 \left(\frac{\alpha}{2\pi} \right) \left(\frac{m\alpha^4}{6n^3} \left[S(S+1) - \frac{3}{2} \right] \delta_{\ell,0} \right) \\
\delta E_n(d) &= -\frac{m^3\alpha^3}{8\pi n^3} \left(c_4^{(1)} S(S+1) \right) \delta_{\ell,0} \\
&= -\left(\frac{m^3\alpha^3}{8\pi n^3} \right) \left(\frac{\alpha}{m} \right)^2 \left(-\ln \left(\frac{\Lambda}{m} \right) + \frac{232}{45} - \ln 2 \right) S(S+1) \delta_{\ell,0} \\
\delta E_n(e) &= -\frac{m^3\alpha^3}{8\pi n^3} \left(c_5^{(1)} [2 - S(S+1)] \delta_{\ell,0} \right) \\
&= -\left(\frac{m^3\alpha^3}{8\pi n^3} \right) \left(\frac{\alpha}{m} \right)^2 \left(-\ln \left(\frac{\Lambda}{m} \right) + \frac{4}{15} - 3\ln 2 + i\pi \right) [2 - S(S+1)] \delta_{\ell,0}
\end{aligned} \tag{19}$$

where n and $\ell = 0$ are the principal and orbital quantum number of the positronium state of interest, and $S = 0$ or 1 is the net intrinsic spin of the e^+e^- state.

Using the formula $\Gamma = -2 \text{Im}(E)$, we obtain from $\delta E_n(e)$ the $O(m\alpha^5)$ decay rate of

the s -wave state of parapositronium ($S = 0$):

$$\Gamma(n, \alpha^5) = \frac{m\alpha^5}{2n^3} \delta_{\ell,0}. \quad (20)$$

In the rest of the paper, we concentrate on the hyperfine splitting so we drop the imaginary part contained in $\delta E_n(e)$. Adding the contributions of diagrams (a), (d) and (e) of Fig. (6), and taking the difference between $S = 1$ and $S = 0$ finally gives:

$$\begin{aligned} \Delta E_{\text{hfs}}(n, \alpha^5) &\equiv \delta E_n(S = 1) - \delta E_n(S = 0) \\ &= - \left(\frac{m\alpha^5}{2\pi n^3} \right) \left[\ln 2 + \frac{16}{9} \right] \delta_{\ell,0}, \end{aligned} \quad (21)$$

in agreement with standard results [6][7].

The hyperfine splitting for arbitrary quantum numbers is computed by modifying the previous calculation in two ways. First, diagram (a) of Fig. (6) must be computed for $\ell \neq 0$ states. Notice that diagrams (d) and (e) of this figure are nonzero only for s -wave states since they represent contact interactions. Secondly, diagrams (b) and (c), which contribute only to $\ell \neq 0$ states, must be computed. Since the calculation of these latter contributions is presented elsewhere [4], we present here just the final result:

$$\Delta E_{\text{hfs}}(n, \ell, \alpha^5) = - \left(\frac{m\alpha^5}{2\pi n^3} \right) \left[\left(\ln 2 + \frac{16}{9} \right) \delta_{\ell 0} - \frac{C_{j\ell}}{4(\ell + \frac{1}{2})} (1 - \delta_{\ell 0}) \right], \quad (22)$$

where j is the total angular momentum quantum number, including electron spin, and the coefficients $C_{j\ell}$ are given explicitly by:

$$C_{j\ell} = \begin{cases} \frac{4\ell+5}{2(\ell+1)(2\ell+3)} & \text{if } j = \ell + 1 \\ -\frac{1}{2\ell(\ell+1)} & \text{if } j = \ell \\ \frac{-4\ell+1}{2\ell(2\ell-1)} & \text{if } j = \ell - 1 \end{cases} \quad (23)$$

To summarize, we see that the hyperfine splitting to $O(m\alpha^5)$ is hardly more difficult to obtain in NRQED than is the $O(m\alpha^4)$ result. The only extra effort required is obtaining the complete matching of all spin-dependent effective operators to next-to-leading order in

α . We have performed the required $O(\alpha^2)$ matchings for those four-fermi operators which had not been previously given in the literature. Furthermore, results for the hyperfine splitting for general n and ℓ are obtained with very little effort.

Acknowledgments

This research was partially funded by the Natural Sciences and Engineering Research Council of Canada. We thank G. Adkins for bringing reference [7] to our attention.

5. References

- [1] W.E. Caswell and G.P. Lepage, *Phys. Lett.* **167B** (1986) 437;
T. Kinoshita and G.P. Lepage, in *Quantum Electrodynamics*, ed. by T. Kinoshita, (World Scientific, Singapore, 1990), pp. 81–89.
- [2] P. Labelle, *Effective Field Theories for QED Bound States: Extending Nonrelativistic QED to Study Retardation Effects*, preprint McGill-96/33 (hep-ph/9608491).
- [3] P. Labelle and S.M. Zebarjad, *Derivation of the Lamb Shift Using an Effective Field Theory*, preprint McGill-96/41 (hep-ph/9611313).
- [4] P. Labelle and S.M. Zebarjad, *An Effective Field Theory Approach to Nonrelativistic Bound States in QED and Scalar QED*, preprint McGill-97/01.
- [5] A. Hoang, P. Labelle and S.M. Zebarjad, work in preparation.
- [6] R. Karplus and A. Klein, *Phys. Rev.* **87** (1952) 848.
- [7] S.Gupta, W. Repko and C. Suchyta III, *Phys. Rev* **D40** (1989) 4100 .
- [8] P. Labelle, *Order α^2 Nonrelativistic Corrections to Positronium Hyperfine Splitting and Decay Rate Using Nonrelativistic Quantum Electrodynamics*, Cornell University Ph.D. thesis, UMI-94-16736-mc (microfiche), Jan 1994.
- [9] M. Nio and T. Kinoshita, *Phys. Rev.* **D53** (1996) 4909.

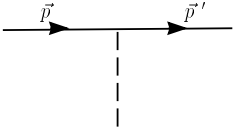
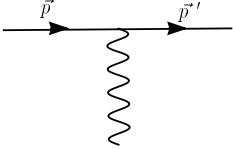
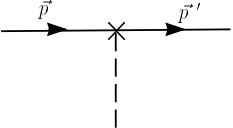
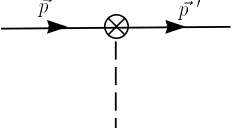
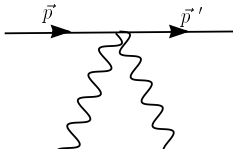
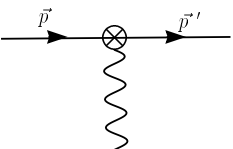
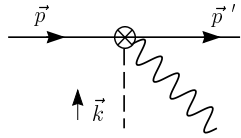
	Coulomb Vertex qe
	Dipole Vertex $-\frac{qe}{2m}(\vec{p}' + \vec{p})$
	Darwin Vertex $-c_2 (\vec{p}' - \vec{p})^2$
	Spin-Orbit Vertex $2 c_3 (\vec{p}' \times \vec{p}) \cdot \vec{\sigma}$
	Relativistic Kinetic Vertex $-\frac{\vec{p}^4}{8m^3}(2\pi)^3\delta^3(\vec{p}' - \vec{p})$
	Seagull Vertex $(qe)^2 \frac{\delta^{ij}}{2m}$
	Fermi Vertex $i c_1 (\vec{p}' - \vec{p}) \times \vec{\sigma}$

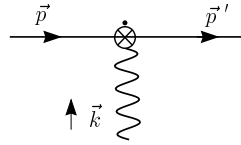
Figure (1)

NRQED Feynman Rules.



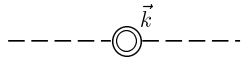
Spin-Seagull Vertex

$$2 q e c_3 \vec{k} \times \vec{\sigma}$$



Time Derivative Vertex

$$-c_3 k^0 (\vec{p} + \vec{p}') \times \vec{\sigma}$$



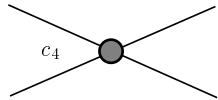
Coulomb Vacuum Polarization Vertex

$$-c_9 \frac{k^4}{m^2} (\delta_{ij} - \frac{k_i k_j}{k^2})$$



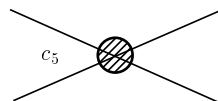
Transverse Vacuum Polarization Vertex

$$c_{10} \frac{k^4}{m^2} (\delta_{ij} - \frac{k_i k_j}{k^2})$$



spin-1 Anihilation Vertex

$$-c_4 \vec{S}^2$$



spin-0 Anihilation Vertex

$$-c_5 (2 - \vec{S}^2)$$

NRQED Feynman (continued).